

## Table of Content

LIST OF ABBREVIATION .....	1
ABSTRACT .....	1
INTRODUCTION.....	3
The NuRD complex and CHD functions .....	3
Snijders Blok-Campeau Syndrome: phenotypes and mechanisms .....	7
iPSCs and the NuRD/CHD3 complex .....	10
Research Aim.....	12
MATERIALS AND METHODS .....	13
RESULTS .....	19
Gene expression analysis demonstrates that <i>CHD3</i> -KO cells are pluripotent .....	19
Protein level expression confirms the pluripotent state of the <i>CHD3</i> -KO iPSC model.....	22
Analysis of surface protein markers further supports the pluripotent state of the <i>CHD3</i> -KO iPSC model .....	23
DISCUSSION .....	24
ACKNOWLEDGEMENTS.....	29
REFERENCES.....	30
SUPPLEMENTARY MATERIALS .....	37

## List of Abbreviation

CHD: Chromodomain Helicase DNA Binding Domain  
CNCC: Cranial Neural Crest Cell  
DUF: Domains of Unknown Function  
ESC: Embryonic Stem Cell  
IF: Immunofluorescence  
iPSCs: induced Pluripotent Stem Cells  
KO: Knocked-Out  
NCC: Neural Crest Cells  
NuRD: Nucleosome Remodeling and Deacetylation  
PHD: Plant Homeodomain  
RNAP II: RNA Polymerase II  
RT-qPCR: Reverse Transcription-quantitative Polymerase Chain Reaction  
scRNA-Seq: single cell-RNA Sequencing  
SNIBCPS: Snijders Blok-Campeau Syndrome  
TF: Transcription Factor  
TPM: Transcripts Per Million  
WT: Wild-Type

## Abstract

The Chromodomain Helicase DNA Binding Domain (CHD3/4/5) proteins are ATPase domain-containing mutually exclusive subunits of the Nucleosome Remodeling and Deacetylation (NuRD) complex. This complex utilizes the ATP hydrolysis energy to remodel chromatin, which regulates downstream transcription. While mutations in *CHD4/5* have been extensively studied, a new

syndrome associated with *CHD3* mutations, known as Snijders Blok-Campeau Syndrome (SNIBCPS), was described in 2018. This syndrome manifests with neurological and craniofacial abnormalities, the latter likely due to impairment of the Cranial Neural Crest Cell (CNCC) differentiation. CNCCs are a transient developmental cell type which arises during embryonic development to give rise to multiple derivatives, including craniofacial bones and cartilage. Despite all the known cases of the syndrome present with *CHD3* genetic mutations, little is known on the role of this protein in embryonic development and there is a lack of *in vitro* studies for SNIBCPS mechanism.

In this study, the induced Pluripotent Stem Cells (iPSCs) with wild-type (WT) and knocked-out (KO) *CHD3* gene are utilized as *in vitro* models. The goal of my project was to investigate whether this *CHD3*-KO iPSC model represents a suitable model to study the function of *CHD3* in iPSC-CNCC differentiation. Specifically, I aimed to investigate if *CHD3*-KO iPSCs retained their pluripotency.

Using a combination of methods: Reverse Transcription-quantitative Polymerase Chain Reaction, bulk RNA-Sequencing analysis, Immunofluorescence, and Flow-Cytometry, I was able to demonstrate that the *CHD3*-KO iPSC model does not exhibit any difference in the expression of the main pluripotency markers comparing with the *CHD3*-WT iPSC model, supporting that this could be a good model to study the role of *CHD3* in CNCC specification.

This research can be continued by further iPSC-CNCC differentiation to investigate potential morphological malformation and differential gene expression of CNCC differentiation markers in the *CHD3* *CHD3*-KO model. In the long run, this research lays groundwork for contributing to SNIBCPS treatment and early diagnostics.

# Introduction

## The NuRD complex and CHD functions

The Nucleosome Remodeling and Deacetylation (NuRD) complex is an evolutionary conserved protein complex being expressed in plants and animals in both developing and developed tissues (Basta & Rauchman, 2015). It is involved in essential biological mechanisms including transcriptional regulation, embryonic development and cerebellar cortex development (Basta & Rauchman, 2015; Torchy, Hamiche & Klaholz, 2015). This complex has two distinct enzymatic activities: ATP-dependent nucleosome remodeling and histone deacetylase activity. Its schematic structure is shown in Figure 1. The MBD2/3 domain bridges the ATPase nucleosome remodeling region, which includes CHD3/4/5 (Chromodomain Helicase DNA Binding Domain), CDK2AP1, GATAD2A/B, with the deacetylase subcomplex, including HDAC1/2, MTA1/2/3, RBBP4/7 (Low et al., 2016; Zhang et al., 2016; Bornelöv et al., 2018).

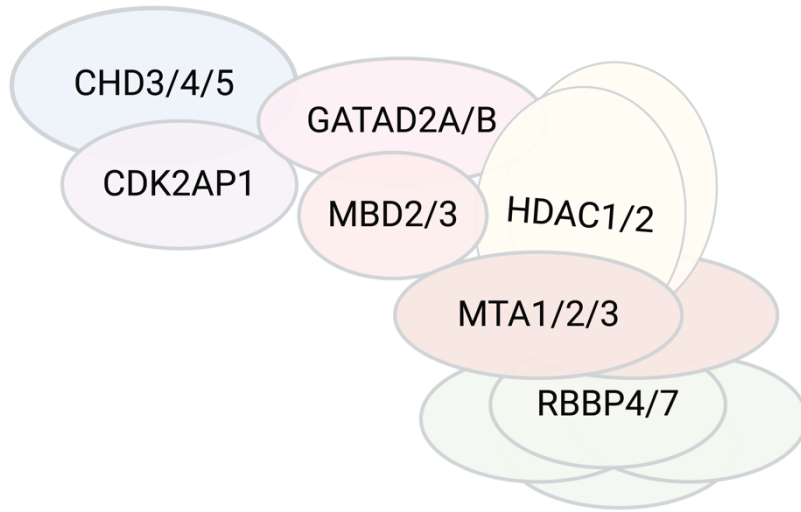


**Figure 1. The NuRD complex structure.** One MBD2/3 protein connects the nucleosome remodeling subcomplex with histone deacetylase subcomplex. The nucleosome remodeling subcomplex comprises of one CHD3/4/5, one CDK2AP1, and one GATAD2A/B protein. Histone deacetylase activity is performed by two HDAC1/2, two MTA1/2/3, and four RBBP4/7 proteins. The NuRD complex structure is adapted from (Bornelöv et al., 2018). The diagram is made by BioRender (BioRender.com, 2024).

CHD is a key component of the NuRD complex, comprising two Plant Homeodomain (PHD) fingers, two tandem chromodomains, one SNF2-like ATPase/helicase domain, domains of unknown function (DUF), and C-terminal 2 domain (Figure 2) (Snijders Blok et al., 2018; Woodage et al., 1997).

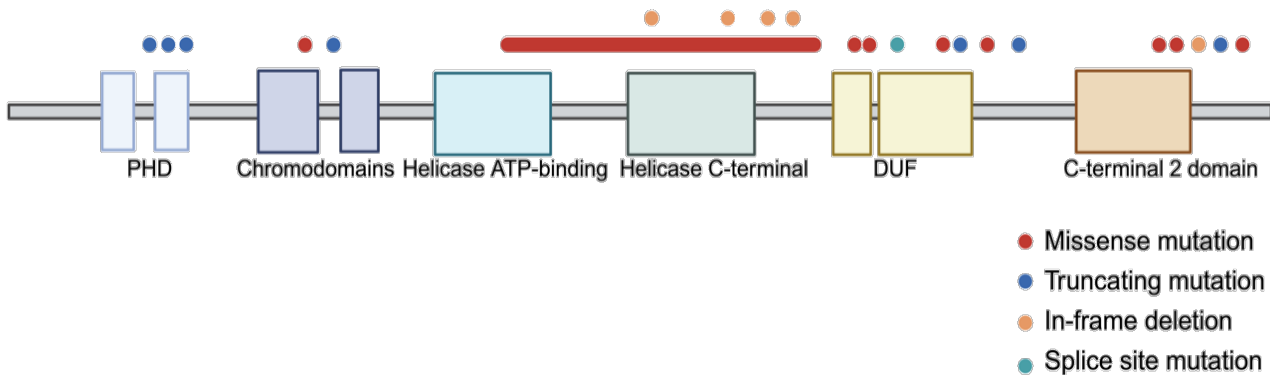


**Figure 2. The CHD protein structure and Snijders Blok-Campeau Syndrome (SNIBCPS) mutation profile on CHD3.** CHD3 is one of the members of the CHD family within the NuRD complex. CHD3/4/5 share the same structure: PHD fingers, Chromodomains, Helicase ATP-binding and C-terminal domains, DUF, and C-terminal 2 domain. The location of color dots and strip are schematic representation of reported site of SNIBCPS mutation. Most mutations are missense mutations and are concentrated within helicase ATP-binding and helicase C-terminal domains. Their colors represent different mutation types, with red represents missense mutation, blue represents truncating mutation, orange represents in-frame deletion, and green represents splice site mutation. PHD: Plant Homeodomain; DUF: Domain of Unknown Function. Protein structure and mutation details are collected from (Snijders Blok et al., 2018; Drivas et al., 2020; Pascual et al., 2023). The diagram is made by BioRender. (BioRender.com, 2024).

Historically, the NuRD complex was considered to be a transcriptional repressor because the histone deacetylase subunit of the NuRD complex are normally involved in repression activity (Xue et al., 1998). The mechanism behind is that histone deacetylases facilitate the removal of acetyl groups from lysine residues on histone proteins. As a result, lysine residues retain their positive charge, allowing histone proteins to bind more tightly to DNA, leading to inhibition of gene transcription (Seto & Yoshida, 2014). However, the view changes as later

research discovered NuRD complex's involvement in both transcriptional repression and activation (Lai & Wade, 2011; Balasenthil et al., 2007).

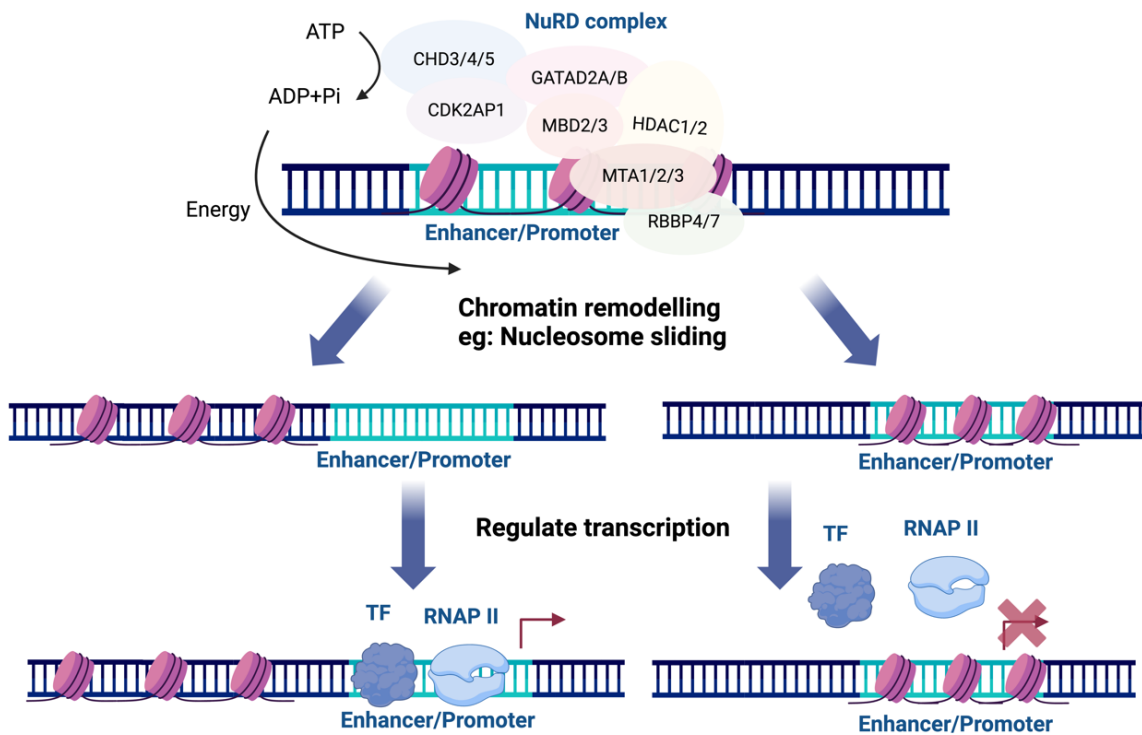


**Figure 3. The NuRD complex functions.** The NuRD complex binds to enhancers and promoters of euchromatic regions. It utilizes the energy released from CHD ATPase hydrolysis to perform nucleosome sliding, which leads to two possible consequences. Left: the euchromatic configuration of the region is kept and exposes the enhancer or promoter for TFs or RNAP II to bind. This can activate the gene transcription. Right: the region switches to heterochromatin nature, which covers the enhancer or promoter for TFs or RNAP II to bind. This activity represses the transcription activity. NuRD complex: Nucleosome Remodeling and Deacetylation complex; TF: Transcription Factor; RNAP II: RNA Polymerase II. The diagram is made by (BioRender.com, 2024).

Global localization data indicates that the NuRD complex has a general affinity to open chromatin (euchromatin) regions, where nucleosomes are loosely packed (Bornelöv et al., 2018). The genome-wide chromatin binding mapping further shows that the NuRD complex can be recruited to almost all enhancers and promoters of Embryonic Stem Cells (ESCs) (de Dieuleveult et al., 2016). The ATPase subunit of CHD can perform hydrolysis, which transfers ATP into ADP

and phosphate. This hydrolytic activity provides energy that the NuRD complex utilizes to facilitate chromatin interactions and remodel nucleosomes, including nucleosome sliding along the DNA sequence (Bornelöv et al., 2018). Utilizing the energy released by the CHD protein, NuRD complex performs chromatin remodeling activity by controlling the nucleosome binding architecture such as sliding the nucleosome along the sequence, possibly by binding the histone 3 subunit of nucleosomes (Musselman et al., 2012). Detailed examples will be discussed in the next paragraph. The remodeling activity leads to two possible consequences. One possibility is that it might keep the euchromatin configuration of the chromosome and ensures accessibility of transcription factors (TFs) or RNA polymerase II (RNAP II) to the transcription initiation sequences such as promoters or enhancers to start the transcription (Figure 3 Left hand side). While the alternative possibility is the euchromatic region becomes heterochromatic, which consist of tightly packed nucleosomes, which prevents TFs and RNAP II to bind and initiate transcription (Figure 3 Right hand side) (Bornelöv et al., 2018; Hoffmann & Spengler, 2019). This transcriptional regulation will impact the downstream cell lineage commitment to ensure CNCC differentiation and the final activities such as craniofacial and neuronal development is successful (Nitarska et al., 2016).

The NuRD complex can comprise one of three homologs of the class II CHD protein: CHD3 (Mi2- $\alpha$ ), CHD4 (Mi2- $\beta$ ), or CHD5. They are mutually exclusive subunits within the complex and are essential in chromatin remodeling activity (Hoffmann & Spengler, 2019). CHD3/4 are expressed ubiquitously while CHD5 is predominantly found in the central nervous system and testis. CHD5 is mainly involved in embryonic neuronal differentiation and neurogenesis (Parenti et al., 2021). CHD4, however, is the most abundant type of CHD protein in the NuRD complex and is the one being extensively researched. It was initially identified as

an autoantigen in dermatomyositis but later research also indicated that it is involved in neuroblast formation (Scimone, Meisel & Reddien, 2010; Wang & Zhang, 2001). In ESCs, CHD4 works to inhibit lineage commitment by repressing transcription of *TBX3*, a gene essential in cell fate determination (Zhao et al., 2017). The capacity of CHD4 and CHD5 to guide the NuRD complex to remodel chromatin remodeling capacity stems from their ability to bind distinct H3 within the same or different nucleosomes (Musselman et al., 2012). For example, CHD5 binds to H3K27me3 (histone H3 trimethylated at Lys 27), an epigenetic modification marker usually for gene repression, to repress nonneuronal genes while CHD4 can bind to H3K4me3 (histone H3 trimethylated at Lys 4), a marker on histone H3 for gene activation, to activate transcription of pluripotency genes (Musselman et al., 2012; Egan et al., 2013). How CHD3 remodel chromatin is currently unknown. Since CHD proteins are homologs, it is plausible that CHD3 remodel chromatin with the same mechanism.

Previous studies found that mutations and deletions within these *CHD* genes are related to a range of human diseases. For example, mutations in *CHD4* are seen in serious endometrial cancer (Le Gallo et al., 2012) while deletion of *CHD5*, which is also a tumor suppressor gene, causes neuroblastomas (Laut et al., 2022). Plausible human disorders related to *CHD3* mutation were unknown until the Snijders Blok-Campeau Syndrome (SNIBCPS) was described.

## **Snijders Blok-Campeau Syndrome: phenotypes and mechanisms**

SNIBCPS, a newly discovered syndrome described in 2018 (Snijders Blok et al., 2018), is an autosomal dominant neurodevelopmental disorder. It is characterized by craniofacial symptoms such as wide-spaced eyes and bossing forehead, along with neurological deficiencies such as speech delay and

intellectual deficiencies (Snijders Blok et al., 2018). Photographs of craniofacial abnormality phenotypes are shown in Figure 4. To date, only 79 SNIBCPS patients have been described. Available datasets indicate mutations in the *CHD3* gene in these SNIBCPS patients, marking the very first syndrome associated with the *CHD3* gene. The majority of patients exhibit heterozygous mutations, with some inherited and most occurring *de novo*. Most patients manifest missense mutation in the helicase domain of *CHD3*, which includes an ATP-binding and a C-terminal domain. Other mutation types observed include in-frame deletions within the helicase domain; missense mutations, splice site variants, in-frame deletions and truncating mutations outside the helicase domain (Figure 2) (Snijders Blok et al., 2018; Drivas et al., 2020; Pascual et al., 2023). There is one case of complete deletion of the *CHD3* gene and one case of 6.5Mb duplication which includes the whole *CHD3* gene (Drivas et al., 2020).



Individual 1

Individual 2

**Figure 4. Photographs of two patients with classical SNIBCPS craniofacial abnormality phenotypes.** Both individual 1 and 2 have wide-spaced eyes, broad forehead, and macrocephaly. Individual 2 also shows low-set ears. Photographs are derived from (Snijders Blok et al., 2018).

The craniofacial abnormalities of the syndrome are putatively caused by the malformation of the Cranial Neural Crest Cell (CNCC) (Siismets & Hatch, 2020). CNCCs are a transient developmental cell type which arises during embryonic development. As shown in Figure 5 black lines, ESCs differentiate into three germ

layers: endoderm, mesoderm, and ectoderm. Next, ectoderm forms the neural tube, from the rostral part of which the CNCCs population arise. These cells undergo epithelial to mesenchymal transition and gain the migratory nature and multipotent. As such, CNCCs can not only differentiate into typical differentiated cells from ectoderm, such as peripheral neurons, but also form cell types which are typically produced from the mesodermal lineage, such as the bone and cartilage of the face (Zalc et al., 2021). Given the marked craniofacial defects, SNIBCPs patients are hypothesized to have dysfunctional CNCC specification.

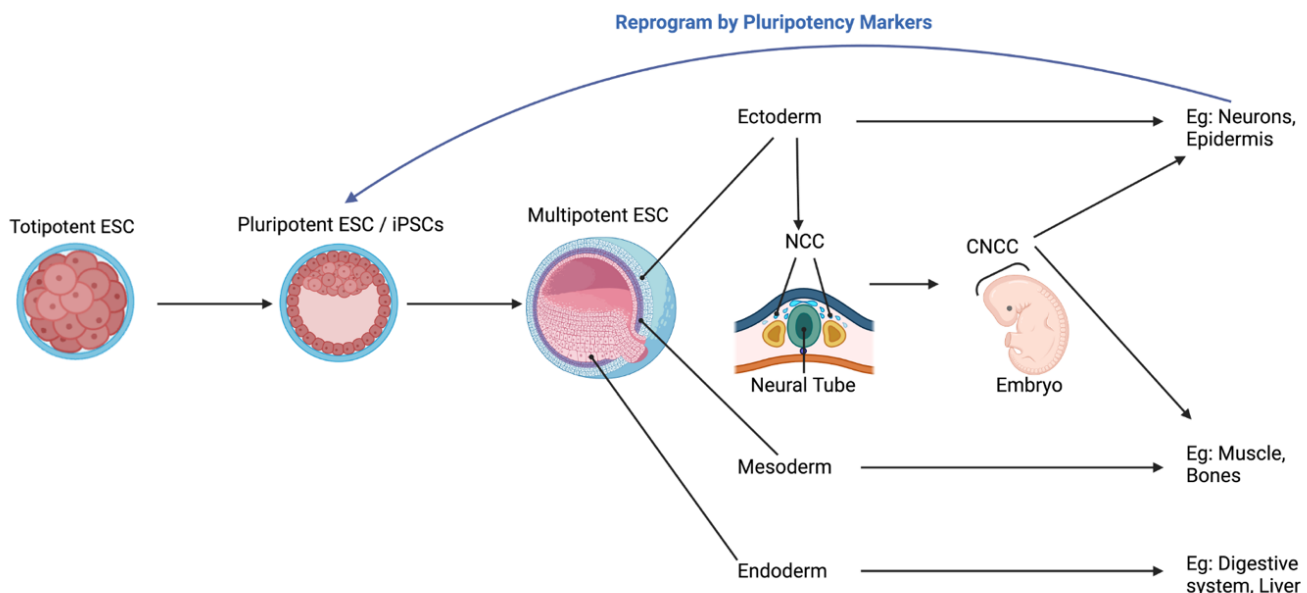


**Figure 5. Representation of the embryonic development and iPSCs production mechanism.** Black lines: The totipotent ESC differentiates into pluripotent ESC, then to multipotent ESC. Multipotent ESC contains three germ layers, which will further differentiate into corresponding somatic cells. Neural tube is derived from ectoderm and will become the spinal cord and the brain of the embryo. The dorsal part of the neural tube are NCCs and the rostral part of which is CNCC, which can undergo epithelial to mesenchymal transition and differentiate into both typically ectoderm and mesoderm-derived cells, such as peripheral neurons, craniofacial cartilages and bones. Blue line: iPSCs technique allows somatic cells to be reprogrammed back to pluripotent ESC-like stage by introducing pluripotency markers. ESC: Embryonic Stem Cell, iPSCs: induced Pluripotent Stem Cells, NCC: Neural Crest Cell, CNCC: Cranial Neural Crest Cell. The diagram is made by BioRender (BioRender.com, 2024).

SNIBCPs patients lack a functional CHD3 ATPase, leading to inadequate energy supply for the NuRD complex to remodel chromatin effectively. Consequently, transcriptional regulation activity may become impaired. This dysfunction may impair CNCC specification and further differentiation into craniofacial derivatives (Bornelöv et al., 2018), which will possibly negatively impact the craniofacial development eventually (Nitarska et al., 2016).

Craniofacial abnormalities impact the formation of head and facial structures which lead to syndromes seen such as wide-spaced eyes, macrocephaly, and broad forehead (Figure 4).

## iPSCs and the NuRD/CHD3 complex

The induced Pluripotent Stem Cells (iPSCs) approach was published by Dr. Shinya Yamanaka and Dr. Kazutoshi Takahashi in 2006 (Takahashi & Yamanaka, 2006). The technique aims to reprogram differentiated somatic cells into undifferentiated pluripotent ESC-like cells, by overexpressing specific pluripotency factors, also known as Yamanaka factors (Figure 5 blue line). The factor cocktail can be OCT4/3, SOX2, C-MYC, KLF4 or OCT4/3, SOX2, LIN28, NANOG (Takahashi & Yamanaka, 2006; Takahashi et al., 2007; Yu et al., 2007). When expressed as TFs, pluripotency factors influence gene expression within somatic cells and activate genes coding for ESC properties (Ye, Swingen & Zhang, 2013). iPSC technique addresses the ethical issue of using real human embryos for stem cell study (King & Perrin, 2014).

To generate iPSCs, Somatic cells can be reprogrammed by introducing integration or integration-free vectors carrying reprogramming factors. Integration vectors, typically retroviruses, insert exogenous genes into the cell genome. However, integration-free vectors, such as episomal vectors, do not require gene

integration into the genome (Yu et al., 2009). Human somatic cells successfully reprogrammed to iPSCs include skin fibroblasts, blood cells and oral mucosa fibroblasts (Takahashi et al., 2007; Ye et al., 2009; Miyoshi et al., 2010).

In this study, iPSCs were used as a model to study the CHD3 deficiency and function as an *in vitro* model for the SNIBCPs. It is crucial to ensure a high level of pluripotency in the model, as only robust pluripotency enables iPSCs to differentiate into various cell lineages, such as CNCCs (Liu & Zheng, 2019). To confirm pluripotency, the teratoma assay is commonly employed, involving the transplantation of iPSCs into immune-compromised mice for subsequent histological analysis of resulting teratomas. It can confirm representation of all three germ layers (Nelakanti, Kooreman & Wu, 2015). However, this method is time-consuming and invasive, which raises ethical and regulatory concerns. Moreover, variations in tumor growth rates and sizes complicate interpretation, potentially reducing specificity for pluripotency assessment. In contrast, in my study, I chose to assess the expression of pluripotency markers at RNA and protein level, offering a rapid, *in vitro* approach. This method provides high specificity and sensitivity, enabling simultaneous assessment of pluripotency levels across the stem cell population.

The core pluripotency factors tested in my study were NANOG, OCT4, and SOX2. They are the most commonly tested core pluripotency factors in ESCs/iPSCs research (Wang et al., 2012). Those pluripotency markers function as intracellular molecules involved in regulating ESC/iPSCs identity and function, surface markers can also be used to identify and characterize ESC/iPSCs based on their physical properties and surface protein expression profiles. The glycolipid SSEA-4 and proteoglycan TRA-1-60-R are important surface markers of ESCs (Lanctot, Gage & Varki, 2007; Takata et al., 2019). In iPSC studies, there is evidence that

fully reprogrammed human iPSCs have strong expression of SSEA-4 and TRA-1-60-R (Pomeroy et al., 2016), indicating that these two markers are the major indicators of iPSCs. Therefore, the expression of these two surface markers was also tested in my project.

The NuRD complex plays a crucial role in ESCs by controlling pluripotency gene expression (Miller et al., 2016). Since iPSC model mimics ESCs, the complex should perform the same function. According to a study, the MBD3 component of the NuRD complex assists the complex to regulate the transcription of pluripotency genes, enabling the translation of functional pluripotency marker TFs in downstream mechanisms (Ee et al., 2017). One study found out that binding of both MBD3 and CHD4 to a promoter/enhancer indicate active transcription of pluripotency factor in mice ESCs (Bornelöv et al., 2018). However, study focusing on the CHD4 component only showed that CHD4 deficient mouse models do not significantly impact the expression of pluripotency genes (Hirota et al., 2019), suggesting that the NuRD complex can maintain its activity in regulating pluripotency even in the absence of CHD4. There is no current research investigating the impact of CHD3 deficiency on pluripotency in human samples, which is identified a knowledge gap worth to investigate in.

## **Research Aim**

SNIBCPS is a newly discovered syndrome, and as such, there is limited research available. Most existing studies are clinical reports, and there is a notable absence of *in vitro* research on this syndrome and the impact of CHD3 deficiency. In this context, this study aims to fill in these knowledge gaps by constructing a feasible iPSC model for *in vitro* SNIBCPS studies, evaluating the pluripotency of the CHD3-KO iPSC model for potential differentiation into CNCCs.

I hypothesized that the *CHD3*-WT and *CHD3*-KO iPSCs exhibit the same level of pluripotency. Four methods were employed to assess the pluripotency level: Reverse Transcription-quantitative Polymerase Chain Reaction (RT-qPCR), bulk RNA-sequencing (RNA-Seq), Immunofluorescence (IF), and Flow Cytometry. This research provides an examination of the iPSC model before further differentiation.

## Materials and Methods

### KO iPSC model construction

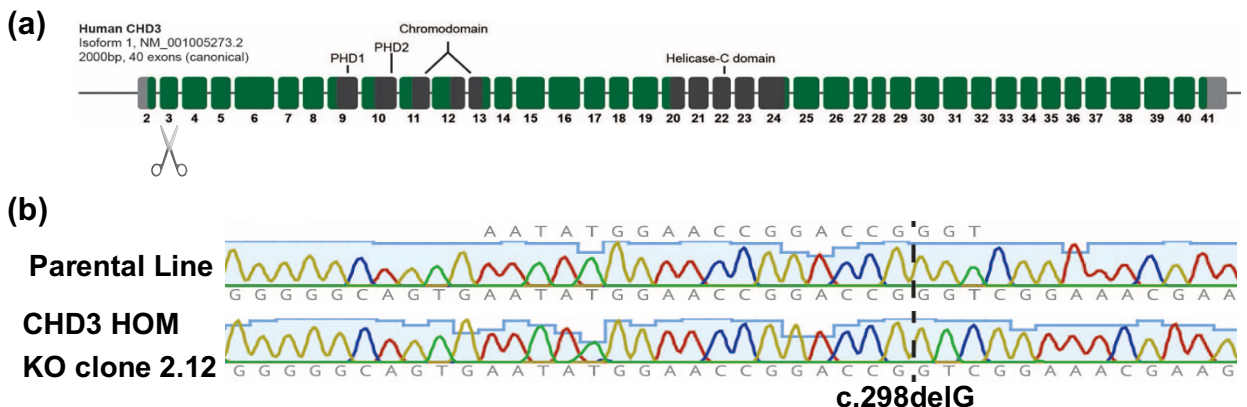


**Figure 6. The representation of the *CHD3* gene structure and the CRISPR-Cas9 KO detail.** (a) The KO occurs at exon 3 of *CHD3*. (b) Quality control by Sanger Sequencing of the *CHD3* HOM KO clone 2.12 made by CRISPR-Cas9 shows a G base deletion at site 298 compared with its parental line. The pictures come from the Dr. Simon Fisher's group of Max Planck Institute.

The BIONi010-A human iPSCs cell line was derived from the human skin fibroblast by skin biopsy (Bioneer, RRID: CVCL\_1E66). The *CHD3*-KO iPSC line *CHD3* HOM KO clone 2.12 was generated by the lab collaborator at the Max Plank Institute, in Netherlands (Dr. Simon Fisher's group). It was generated by CRISPR-Cas9 editing of the BIONi010-A line (Max Planck Institute). A homozygous base deletion (c.298delG, NM\_00005273.2) was made to the exon

3 and a frameshift is generated, which causes an early stop codon (p.G100Vfs\*40) to be generated in the transcribed mRNA. The KO detail is shown in Figure 6.

### **iPSCs culture**

Each new plate for cell passage was prepared with DMEM (Gibco, A4192002) containing 1% Geltrex matrix (Thermo Fisher Scientific, A1413302). The manufactured iPSCs started at passage 30. The iPSCs cell line was being passaged every 3-4 days when there was ~70% confluency, using 1mL EDTA (Fisher Scientific, 11836714) for cell detaching. mTeSR plus (Stem Cell Technologies, 100-0274 and 100-0275) containing 1% Penicillin-Streptomycin (Pen-Strep) mixture (Gibco, 15070063) was used for maintenance. Medium was changed every 1-2 days when there was <50% confluency, using mTeSR plus with 1% Pen-Strep mixture only. Before each pluripotency assessment experiment, cells from the cell culture were separated into a new plate and grown until the required condition was achieved.

### **Reverse Transcription-quantitative Polymerase Chain Reaction (RT-qPCR)**

The iPSCs should be highly confluent (~90%) before detachment. The iPSCs (*CHD3*-WT/*CHD3*-KO) were detached from plates by accutase (Gibco, A1110501) which is a strong buffer for cell detaching (Lai et al., 2022). Disassociated cells were centrifuged and only cell pellets were kept. Three biological repeats were made for *CHD3*-WT and *CHD3*-KO iPSCs samples. RNA was extracted following the Monarch Total RNA Miniprep Kit (New England Biolabs, #T2010S) protocol. The RNA concentration (ng/μL) was assessed by the NanoDrop Microvolume Spectrophotometer (Thermo Fisher Scientific, ND-1000).

RNA samples were reverse transcribed into cDNA using Maxima First Strand cDNA Synthesis Kit for RT-qPCR (Thermo Fisher Scientific, #K1641) protocol. The conversion includes preparing a 20 $\mu$ L mix of 600ng RNA samples, 4 $\mu$ L 5X reaction mix, 2 $\mu$ L maxima enzyme mix, and nuclease free water. Next, samples were incubated on the heatblock (Thermo Fisher Scientific, 13687712) for 10 minutes at 25°C, 15 minutes at 50°C, and the reaction was terminated by heating for 5 minutes at 85°C.

To prepare for qPCR, master mixes of forward and reverse primers (Thermo Fisher Scientific, 10336-022. The sequences are listed in Table1.), SYBR Green (Applied Biosystems, A25741), and water were made for 18s rRNA, CHD3, NANOG, OCT4 and SOX2 biological and technical replicates respectively. For each biological replicate, three technical replicates were made. 7.5 $\mu$ L of master mix and 2.5 $\mu$ L of diluted cDNA were added to each well of 96-well PCR plates for reaction. The well plate was read by the qPCR machine (Bio-Rad Laboratories, CFX Connect Real-Time PCR Detection System) for 1 hour 26 minutes. The cycling conditions were as follows: initial denaturation at 95°C for 3 minutes, followed by 40 cycles of denaturation at 95°C for 10 seconds, annealing at 63°C for 20 seconds, and extension at 72°C for 30 seconds. Fluorescence signal acquisition occurred during the annealing/extension step.

The raw threshold cycle value (Cq) was recorded by the machine. The fold change in gene expression for CHD3, NANOG, OCT4 and SOX2 (target genes) for both CHD3-WT and CHD3-KO samples were calculated by the Livak-Schmittgen method (Ganger, Dietz & Ewing, 2017). The RNA level was normalized using the 18s rRNA. The statistical test applied was the unpaired t-test assuming equal variance. One-tail test was used for CHD3 only, while two-

tail analysis was applied to all pluripotency genes. The 95% confidence interval was also calculated.

**Table 1. List of the forward and reverse primer sequences for the qPCR experiment**

Gene	Forward (5'-3') sequence	Reverse (5'-3') sequence
18s rRNA	ATACATGCCGACGGCGCTG	AGGGGCTGACCGGTTGGTT
CHD3	AGGAAGACCAAGACAACCAGTCAG	TGACTGTCTACGCCCTTCAGGA
NANOG	ATGCCTCACACGGAGACTGT	AAGTGGGTTGTTGCCTTG
SOX2	GCCGAGTGGAAACTTTGTCG	GCAGCGTGTACTTATCCTTCTT
OCT4	TCGAGAACCGAGTGAGAGG	GAACCACACTCGGACCACA

### Immunofluorescence (IF)

Preparation for IF required transferring the *CHD3*-WT and *CHD3*-KO iPSCs to 12-well plates with coverslips, with three wells for negative control (only secondary antibody is added) and three wells for tested samples (both primary and secondary antibodies are added) for each plate. The iPSCs should form small colonies before fixing. iPSCs were fixed by 4% formaldehyde (4mL 37% formaldehyde (Fisher Scientific, 10532955) dilute with 36mL PBS) in 37°C incubator for 15 minutes. The samples were permeabilized with 0.1% Triton-X100 (Merck Millipore, 648463-50ML) for 10 minutes at room temperature, followed by blocking in 10% Donkey Serum (Abcam, AB7475) for 1 hour at room temperature.

Primary antibodies 0.2% Rabbit SOX2 Polyclonal Antibody (Cambridge Bioscience, Cat# 39843, RRID: AB\_2750954), 2% Goat OCT4 Polyclonal antibody (Bio-Techne, Cat# AF1759, RRID: AB\_354975), and 2% Goat NANOG Polyclonal Antibody (Bio-Techne, Cat# AF1997, RRID: AB\_355097) were added

to the corresponding tested samples. Staining happened overnight on the rocker (Stuart Scientific, Platform Shaker STR6) at 4°C. Secondary antibodies 0.2% Donkey Polyclonal Anti-Rabbit Alexa Fluor 488 Antibody (Life Technologies, Cat# A32790, RRID: AB\_2762833) and 0.2% Donkey Polyclonal Anti-Goat Alexa Fluor 594 Antibody (Life Technologies, Cat# A11058, RRID: AB\_2534105) were added to both tested and negative controls. 1µg/mL of DAPI (BioLegend, Cat# 422801) was added to each sample well.

Prepare slides mounted with coverslips. Slides were kept in the dark at room temperature overnight. Widefield microscopy (40X magnification) (Zeiss, Axio Observer) was used for microscopy. The NANOG and OCT4 TFs were revealed by 594nm wavelength, while SOX2 was revealed by 488nm wavelength.

### **Flow Cytometry**

The experiment followed (Pagliaroli et al., 2021) protocol. *CHD3*-WT and *CHD3*-KO iPSCs were prepared separately in advance. Accutase (Gibco, A1110501) was used to detach cells when high confluency was achieved. PBS-2% Fetal Bovine Serum (Gibco, A1110501) was used to wash nucleated cells. Cell number was examined by the Countess Cell Counter (Invitrogen, Countess II).

For each sample, 1 million cells were added and stained with specific antibodies, including 4µL of TRA-1-60-R PE (BioLegend, Cat# 330609), 2µL of SSEA-4 APC (BioLegend, Cat# 330417) and 1µL of DAPI (BioLegend, Cat# 422801). Fully stained samples required all three antibodies while unstained samples served as control. A sample with only DAPI added was prepared for background control. Samples that compensated for spectral overlap between TRA-1-60-R PE, SSEA-4 APC, and DAPI were also prepared. Single color fluorescence controls, consisting of antibody binding compensation beads (Invitrogen, 01-3333-41) with

either TRA-1-60-R PE or SSEA-4 APC, were prepared. Samples were incubated with antibodies for 15 minutes on ice in darkness.

Set the flow cytometer machine (Agilent Technologies, 2010284AA NovoCyte Penteon U7V7B6Y6R4 Flow Cytometer System) laser wavelength corresponding to each fluorophore: PE (561nm), APC (637nm), DAPI (405nm). 10,000 events were collected per sample. Compensation was performed using DAPI and single-color fluorescence controls, with spectral overlap compensation conducted as needed. The fully stained and unstained samples for both *CHD3*-WT and *CHD3*-KO iPSC models were tested.

FlowJo (version 10.10.0) was applied for data analysis. The same gating strategies were applied to all samples. Gating involved gating cell of interest (FSC-A vs SSC-A), single cells (FSC-A vs FSC-H), live cells (FSC-A vs DAPI-A), and cells expressing surface proteins (PE-A vs APC-A).

### **RNA-Sequencing dataset**

The sequenced samples were prepared by Ms. Zoe Mitchell. Three *CHD3*-WT and three *CHD3*-KO repeats were prepared. The RNA-Sequencing was carried out by the Wistar Institute. The adaptors were removed by TrimGalore! ([https://www.bioinformatics.babraham.ac.uk/projects/trim\\_galore/](https://www.bioinformatics.babraham.ac.uk/projects/trim_galore/)). Then Kallisto program (Bray et al., 2016) was used to align the sequences and generated a dataset applied with TPM (Transcripts Per Million) normalization method. This raw data was transformed by log2.

### **Statistical Analysis**

F-test was applied to all datasets to assess whether their variances are equal. If the variance is equal, unpaired Student's t-test assuming equal variance was conducted. Conversely, if the variance was unequal, unpaired Student's t-test assuming unequal variance was conducted. Whether one tail or two tail analysis should be conducted was based on specific scenario.

## Results

### Gene expression analysis demonstrates that *CHD3*-KO cells are pluripotent

Understanding the gene expression levels of the main pluripotency markers (NANOG, OCT4, SOX2) is crucial for understanding the pluripotency level of the iPSC models as they need to be successfully expressed to translate into TFs.

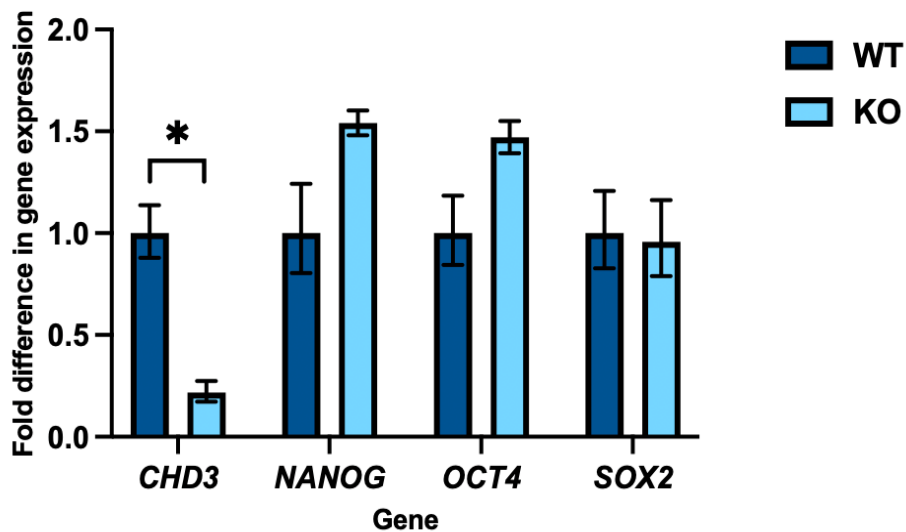


**Figure 7. RT-qPCR result for the fold change in gene expression for *CHD3*-WT and *CHD3*-KO iPSC models.** *CHD3*-KO model shows significantly lower fold difference in *CHD3* gene expression but displays similar gene expression level of pluripotency genes as *CHD3*-WT. 18s rRNA was used for RNA level normalization. Unpaired Student's t-test with equal variance assumption was applied. Two-tail analysis was applied except *CHD3*, \* $p<0.01$ . Dark blue represents *CHD3*-WT iPSC model while light blue represents *CHD3*-KO iPSC model.

To assess the pluripotency at the genetic level, RT-qPCR analysis was conducted using RNA extracted from *CHD3*-WT and *CHD3*-KO iPSCs (Figure 7). The gene expression level of *CHD3* was also tested to confirm the *CHD3*-KO. As expected, the qPCR showed a significantly lower expression of the *CHD3* gene in the *CHD3*-KO model compared to the *CHD3*-WT, confirming the success of the CRISPR-Cas9 knockout performed by our collaborators.

Importantly, no statistically significant difference was detected between *CHD3*-KO and *CHD3*-WT in the expression of the three tested pluripotency genes. Given that the *CHD3*-WT line serves as a reference for normal pluripotency, this suggests that the *CHD3*-KO model retains a normal degree of pluripotency.

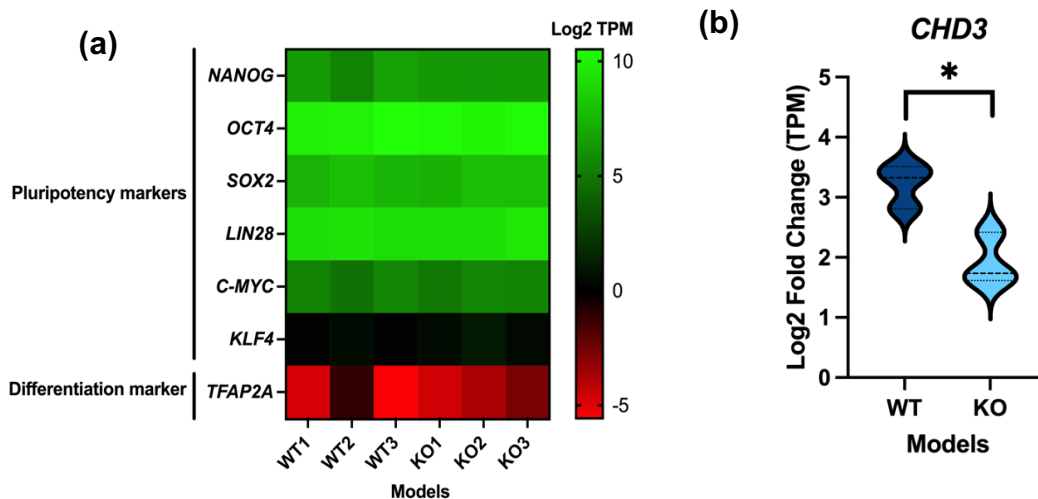


**Figure 8. The RNA-Seq gene expression profile in *CHD3*-WT and *CHD3*-KO iPSC models.** (a) Gene expression heatmap for pluripotency markers and CNCC differentiation marker. All pluripotency markers are highly expressed, whereas differentiation marker shows low expression. Highly expressed genes are represented in green, while lowly expressed genes are shown in red. (b) Log<sub>2</sub> fold change (TPM) of *CHD3* gene expression. *CHD3*-WT model reveals a significantly higher expression than *CHD3*-KO model. Statistical analysis conducted was the Unpaired Students' t-test assuming equal variance. One-tail analysis was applied, \*p<0.01. Dark blue represents *CHD3*-WT iPSC model while light blue represents *CHD3*-KO iPSC model. TPM was the normalization method applied for relative abundance of transcripts in the reads.

RT-qPCR analysis can only test the selected genes' expression since specific primers were used. To comprehensively test the pluripotency levels of the *CHD3*-KO line, the expression of other pluripotency genes and differentiation markers were tested by bulk RNA-Seq analysis (Figure 8).

I checked for the expression profiles of all the main pluripotency markers: *OCT4* and *LIN28* are the most highly expressed pluripotency genes for both *CHD3*-WT and *CHD3*-KO models while *NANOG*, *SOX2*, and *C-MYC* exhibit lower but still considerable expression levels in both models. *KLF4*, however, displays minimal expression in all models, despite being a pluripotency marker (Figure 8(a)). This will be further explained in the discussion section. There is no significant difference in expression levels between *CHD3*-WT and *CHD3*-KO models for any of the pluripotency markers, indicating no differential expression as indicated by the heatmap and t-test statistical analysis (Supplementary Figure 1). In addition, as expected, the CNCC differentiation marker *TFAP2A* is not highly expressed in either *CHD3*-KO or *CHD3*-WT samples. Overall, these data suggest that both models are fully reprogrammed iPSCs with adequate pluripotency.

As expected (and as noted already via RT-qPCR), the *CHD3* gene expression analysis shows a significant decrease in the *CHD3*-KO model compared to *CHD3*-WT ( $p<0.01$ ) (Figure 8(b)). In addition, only a small number of *CHD3* genes in the *CHD3*-KO iPSC model (91 genes) is found as differentially expressed. This supports that *CHD3*-KO minimally affects the transcriptome of the iPSCs, making them a suitable model for differentiation experiments.

No changes in expression of the *CHD4/5* genes are detected, suggesting that the *CHD3*-WT iPSCs do not compensate to the *CHD3* loss by upregulating other

*CHDs* (Supplementary Figure 1(c)). Further detail will be discussed in the discussion section.

### Protein level expression confirms the pluripotent state of the *CHD3-KO* iPSC model

The pluripotency markers will translate into protein (TFs) following successful gene expression. In the protein form, they regulate genes crucial for ESCs/iPSCs cell maintenance. Therefore, assessing pluripotency levels at the protein level is central to understand whether both models are suitable for further differentiation.

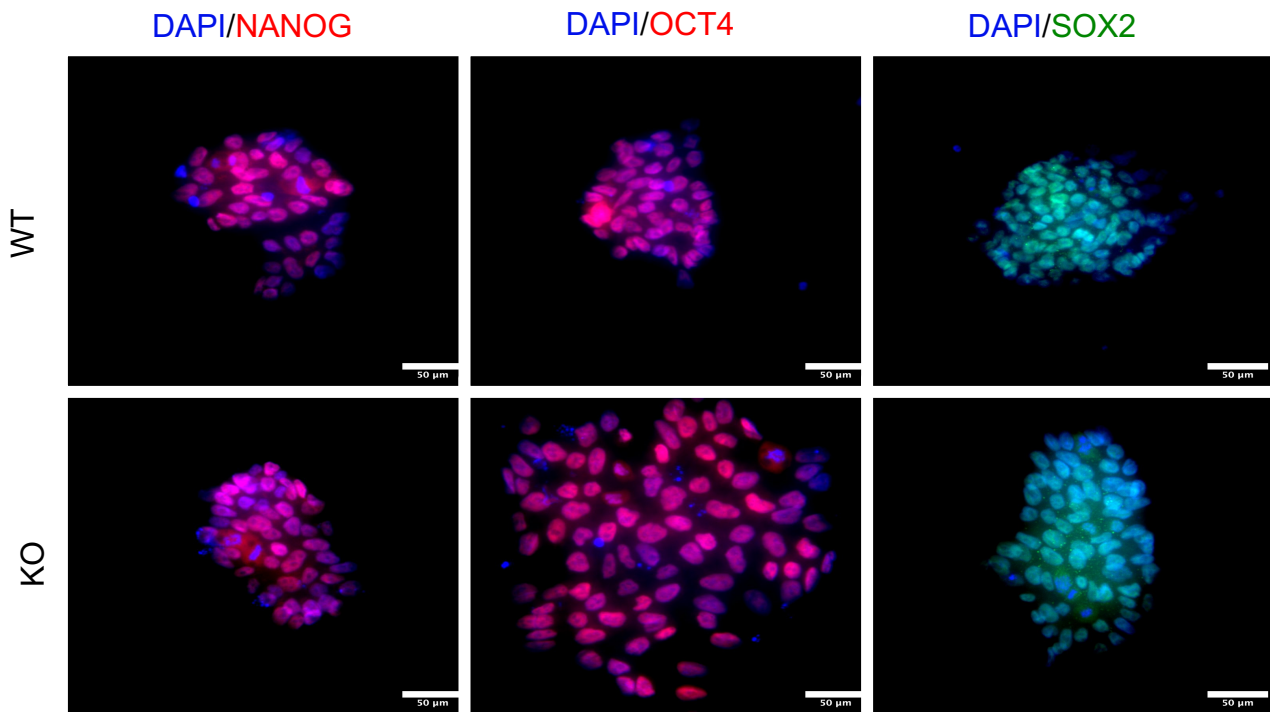


**Figure 9. The IF images for the pluripotency marker TFs for *CHD3-WT* and *CHD3-KO* iPSC models.** There is no significant difference between *CHD3-WT* and *CHD3-KO* iPSC models in terms of fluorescence intensity. Primary and secondary antibodies were used to bind and amplify each pluripotency marker TF respectively. Nuclei were stained with DAPI (blue). NANOG (red), OCT4 (red), SOX2 (green) were visualized by corresponding antibodies tagged with fluorophores. Images were captured by Widefield Microscopy (40X magnification). Scale bar represents 50 $\mu$ m.

The expression level of the three main pluripotency TFs (SOX2, OCT4, NANOG) were visualized via IF using corresponding primary and secondary antibodies for the IF experiment, as shown in Figure 9.

The result indicates high protein level expression for all the three TFs, with no discernible difference between *CHD3*-WT and *CHD3*-KO models in terms of the fluorescence staining patterns of all pluripotency TFs, which indicates that the *CHD3*-KO iPSCs exhibit strong expression of pluripotency markers. This suggests that *CHD3*-KO iPSC model exhibit sufficient pluripotency.

### **Analysis of surface protein markers further supports the pluripotent state of the *CHD3*-KO iPSC model**

Surface protein markers play a crucial role in defining the identity and state of iPSCs, and their expression levels can provide valuable insights into cell property.

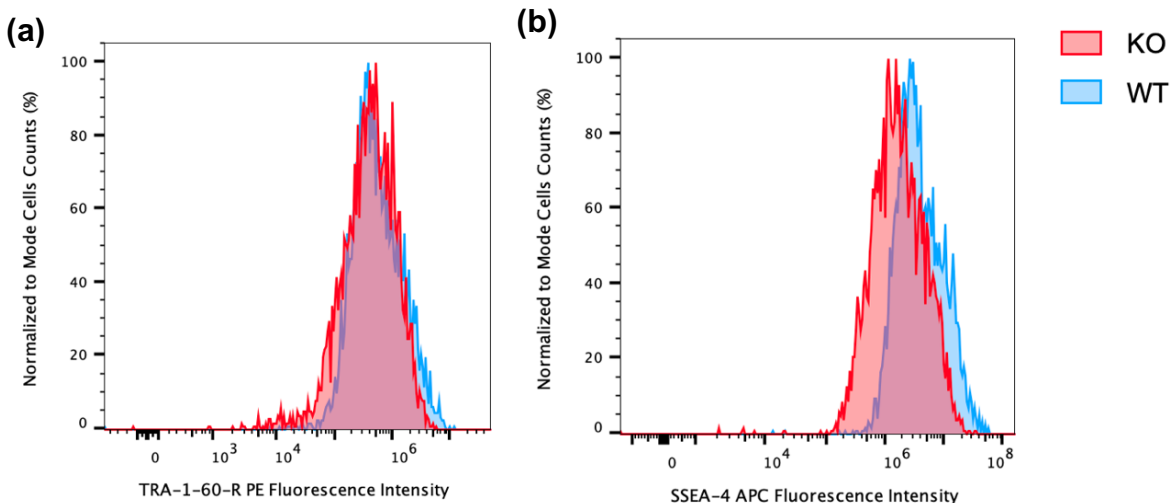


**Figure 10. The cell counts (%) for different fluorescence intensity of surface markers.** (a) The TRA-1-60-R PE, (b) SSEA-4 APC. There is a high degree of overlap between the *CHD3*-WT and *CHD3*-KO model histograms for both markers. The y-axis shows the number of cells that fall within each fluorescence intensity "bin". The peak represents the most common intensity level for that marker among the cells analyzed. The diagrams are normalized to mode. Red represents *CHD3*-KO iPSC model while blue represents *CHD3*-WT iPSC model.

Commonly tested surface markers are SSEA-4 and TRA-1-60-R, which can be fluorescent after being tagged by fluorophore APC and PE respectively. The fluorescence intensity was tested by flow cytometry (Figure 10).

For TRA-1-60-R PE, there is no difference between the *CHD3*-WT and *CHD3*-KO iPSC model (Figure 10(a)). This suggests that the majority of the cells in both models have comparable expression levels for this marker. For SSEA-4 APC, a slight, but not significant, shift of the peak of fluorescence intensity for this protein in the *CHD3*-KO model is detected (Figure 10(b)), indicating that *CHD3*-KO iPSCs express slightly less SSEA-4 relative to the *CHD3*-WT line. Nonetheless, there is still a great overlap between the SSEA-4-expressing cell populations in *CHD3*-WT and *CHD3*-KO models, showing that there is no major difference between the two models.

In conclusion, gene and protein expression analyses confirmed that the *CHD3*-WT and *CHD3*-KO iPSC models show no difference in terms of pluripotency, hence supporting the CRISPR-Cas9 edited *CHD3*-KO iPSCs as a suitable model to conduct further differentiation experiments.

## Discussion

Snijders Blok-Campeau syndrome (SNIBCPS), a newly discovered neurodevelopmental syndrome, has only been characterized by a few reports detailing patient symptoms and the mutated gene, *CHD3* (Snijders Blok et al., 2018; Drivas et al., 2020; Pascual et al., 2023). However, there is a lack of *in vitro* studies to understand its underlying mechanisms. *In vitro* studies offer controlled conditions and eliminate ethical concerns associated with embryonic research

(King & Perrin, 2014). iPSCs, which mimic the ESCs (Takahashi & Yamanaka, 2006), is an ideal model for studying this developmental syndrome. However, to comprehensively capture the disorder's progression, a feasible model with sufficient pluripotency must be constructed to facilitate subsequent differentiation. In this study, I compared the *CHD3*-KO iPSC model with the *CHD3*-WT iPSC model (isogenic) on gene expression level, TFs protein expression level, and surface protein expression level to demonstrate that the *CHD3*-KO model has a similarly high level of pluripotency just as in the *CHD3*-WT model and is ready for further differentiation.

Therefore, I hypothesize that CHD3 deficiency does not impact the pluripotency of the ESCs/iPSCs. Since CHD proteins exist mutually exclusive inside the NuRD complex, it is likely that if CHD3 is deficient, the NuRD complex with CHD4/5 subunit can still regulate the pluripotency as normal (Hoffmann & Spengler, 2019).

Both RT-qPCR and RNA-Seq analysis reveal that *CHD3* is being downregulated in the *CHD3*-KO iPSC model (Figure 7, Figure 8(b)). Although according to the Sanger Sequencing, the CRISPR-Cas9 knock-out for the *CHD3*-KO model is successful (Figure 6 (b)), the expression of the *CHD3* in the *CHD3*-KO model is not zero. This is because CRISPR-Cas9 knock-out cannot achieve 100% modification success rate. A certain amount of iPSCs in the *CHD3*-KO model do not have their *CHD3* gene being edited properly (Lu et al., 2023), which will continue to express this gene normally. However, most shortened mRNA transcript being produced after successful CRISPR-Cas9 edit undergo degradation by the nonsense-mediated mRNA decay (NMD) pathway. NMD can degrade mRNA containing premature termination codon (PTCs), such as the early stop codon introduced in the *CHD3*-KO model, by exoribonuclease enzyme

XRN1 (Brogna & Wen, 2009). Consequently, the expression level of CHD3 in the *CHD3*-KO model remains relatively low.

Both RT-qPCR and RNA-Seq show comparable expression levels of core pluripotency markers, *NANOG*, *OCT4*, and *SOX2*, in both the *CHD3*-WT and *CHD3*-KO models (Figure 7, Figure 8(a)). The RNA-Seq further demonstrates high expression levels of these core pluripotency markers, along with *LIN28* and *C-MYC*, in both models (Figure 8(a)). While *KLF4* is considered a pluripotency marker (Takahashi & Yamanaka, 2006), it does not exhibit high expression in the RNA-Seq heatmap (Figure 8(a)). This discrepancy is attributed to the fact that *KLF4* is more highly expressed in pre-implantation naïve blastocyst than post-implantation primed epiblast ESC, whereas iPSCs simulate the latter stage (Huang et al., 2020). Therefore, *KLF4* is not strongly expressed in iPSCs, which explains the reason that it does not show high expression in the RNA-Seq data.

The only paper available that discusses CHD3, CHD4, and CHD5 deficiency is based on mouse ESC models and it shows that when depleting CHD3, CHD5 can compensate for some CHD3 functions such as driving neuronal migration (Nitarska et al., 2016). However, from the RNA-Seq data, there is no significant upregulation of the *CHD4* or *CHD5* gene expression in the *CHD3*-KO model which shows no sign of compensation (Supplementary Figure 1(c)). This can be explained by two possibilities. One is the fact that CHD3 might play a very specific role that is unknown currently in the iPSCs that other CHD proteins such as CHD5 cannot compensate. The second reason could be that since *CHD3* is very lowly expressed in iPSCs even in the *CHD3*-WT model (Figure 8(b)), knocking out this gene does not make it necessary for other CHD proteins to compensate its role, as CHD3 is likely dispensable at this stage. The compensation does not seem to happen at such an early stage of development.

RNA-Seq can capture the bulk gene expression level, which provides a larger picture than the RT-qPCR. However, the pluripotency gene expression of every cell might vary and it is possible that there will be differences between the *CHD3*-WT and *CHD3*-KO models in terms of the percentage of cells fully express the pluripotency genes (Chen et al., 2020). Alternatively, single cell RNA-Sequencing (scRNA-Seq) is able to quantify the transcriptome of every cell (Chen et al., 2020).

The IF experiment shows similar level of fluorescence intensity of three pluripotency marker TFs in *CHD3*-WT and *CHD3*-KO models, indicating similar expression level (Figure 9). However, this experiment is limited by its qualitative nature. Although the Fiji software can measure the fluorescence intensity (Shihan et al., 2021), it is difficult to measure and compare the intensity of every cell. Mass spectrometry based proteomics, however, can quantify TF expression levels at the protein level by measuring peptide abundance (Simicevic & Deplancke, 2017).

I observed that the surface protein markers SSEA-4 and TRA-1-60-R are significantly expressed in both *CHD3*-WT and *CHD3*-KO iPSC models indicating sufficient pluripotency for both (Figure 10). However, SSEA-4 fluorescence intensity does not show a full overlap between two models (Figure 10(b)). This might not represent the real situation because only one repeat was done. However, more surface proteins could be examined to determine if the *CHD3*-KO model iPSCs are biologically the same as the *CHD3*-WT. Shown by high-throughput flow cytometry, other surface proteins expressed on human ESCs surface include SSEA-3, TRA-1-81, PDPM, and CD24 (Collier et al., 2017). These markers can potentially be expressed on iPSCs too. Further investigation into different types of surface proteins can give a full picture of the surface protein expression profile.

While the homozygous *CHD3*-KO iPSC model used in this study effectively represents a functional *CHD3* deficiency, it does not fully capture the genetic profile observed in the majority of SNIBCPS patients, which often involves heterozygous missense mutations (Snijders Blok et al., 2018). Furthermore, the symptoms such as craniofacial abnormalities are putatively caused by CNCC malformation (Siimets & Hatch, 2020), which necessitates further differentiation of iPSCs.

Given the technical challenges associated with constructing a missense mutation model using CRISPR-Cas9, the next step could start with exploring the cell morphological and expression of differentiation markers such as *TFAP2A* and *NR2F1* differences between the *CHD3*-WT and *CHD3*-KO iPSC models after differentiation into CNCCs (Prescott et al., 2015). The differentiation process involves initially committing iPSCs to the neuroectoderm lineage, followed by CNCC differentiation. A protocol made by Prescott et al. (2015) can be considered. Details of this protocol is shown in Supplementary Figure 2. This protocol operates by inhibiting the TGF- $\beta$  family at an early stage and activating the Wnt and BMP pathways later on. The TGF- $\beta$  family is known to maintain pluripotency while repressing differentiation genes (Temple, 2001), with FGF and EGF factors in the differentiation media capable of repressing this pathway (Watabe & Miyazono, 2009). Additionally, the Wnt pathway activator ChiRON (Turner et al., 2014) is included in later maintenance media to promote CNCC differentiation. While BMP signals maintain pluripotency at the ESC stage, they induce neural crest cell differentiation and repress pluripotency genes in later embryonic development (Watabe & Miyazono, 2009). BMP2, highly expressed in craniofacial skeletal development (Beederman et al., 2013), is included in the late maintenance medium to facilitate CNCC commitment.

In the long run, this study serves as a foundational step in investigating the role of CHD3 in embryonic development, an aspect often overlooked in CHD protein research. In addition, by revealing the mechanism behind, it paves the way for more advanced *in vitro* and *in vivo* studies to enhance our understanding of SNIBCPs. For instance, iPSC-derived cerebral organoids can mimic brain development and elucidate the mechanism of how mutations lead to progressive language delays in some patients (Lancaster & Knoblich, 2014). Additionally, *in vivo* studies in mouse models can unveil the entire developmental process of SNIBCPs from embryo to birth. Eventually, a comprehensive understanding of the underlying mechanism may facilitate the development of targeted therapies or genetic screening methods.

## Acknowledgements

Firstly, I would like to express great thankfulness to Dr. Marco Trizzino for intriguing my interest in the iPSC research during the Stem Cells, Regeneration, and Ageing lecture. It is the most extraordinary technique I have ever learned. I would like to thank Dr. Marco Trizzino and Ms. Zoe Mitchell for all the meticulous support throughout my project, as well as feedback on my poster and report. I would also like to thank other members in the lab: Ms. Martina Demurtas and Dr. Laura Deelen for providing me with additional support throughout the project.

Also, I would like to thank Dr. Simon Fisher's group from Max Plank Institute in Netherlands for providing us with the CHD3 HOM KO clone 2.12 iPSC cell line.

## References

- Balasenthil, S., Gururaj, A.E., Talukder, A.H., Bagheri-Yarmand, R., Arrington, T., Haas, B.J., Braisted, J.C., Kim, I., Lee, N.H. & Kumar, R. (2007) Identification of Pax5 as a Target of MTA1 in B-Cell Lymphomas. *Cancer Research*. 67 (15), 7132–7138. doi:10.1158/0008-5472.CAN-07-0750.
- Basta, J. & Rauchman, M. (2015) The nucleosome remodeling and deacetylase complex in development and disease. *Translational Research*. 165 (1), 36–47. doi:10.1016/j.trsl.2014.05.003.
- Beederman, M., Lamplot, J.D., Nan, G., Wang, J., Liu, X., et al. (2013) BMP signaling in mesenchymal stem cell differentiation and bone formation. *Journal of biomedical science and engineering*. 6 (8A), 32–52. doi:10.4236/jbise.2013.68A1004.
- Bornelöv, S., Reynolds, N., Xenophontos, M., Gharbi, S., Johnstone, E., Floyd, R., Ralser, M., Signolet, J., Loos, R., Dietmann, S., Bertone, P. & Hendrich, B. (2018) The Nucleosome Remodeling and Deacetylation Complex Modulates Chromatin Structure at Sites of Active Transcription to Fine-Tune Gene Expression. *Molecular Cell*. 71 (1), 56-72.e4. doi:10.1016/j.molcel.2018.06.003.
- Bray, N.L., Pimentel, H., Melsted, P. & Pachter, L. (2016) Near-optimal probabilistic RNA-seq quantification. *Nature Biotechnology*. 34 (5), 525–527. doi:10.1038/nbt.3519.
- Brogna, S. & Wen, J. (2009) Nonsense-mediated mRNA decay (NMD) mechanisms. *Nature Structural & Molecular Biology*. 16 (2), 107–113. doi:10.1038/nsmb.1550.
- Chen, T., Li, J., Jia, Y., Wang, J., Sang, R., Zhang, Y. & Rong, R. (2020) Single-cell Sequencing in the Field of Stem Cells. *Current Genomics*. 21 (8), 576–584. doi:10.2174/1389202921999200624154445.
- Collier, A.J., Panula, S.P., Schell, J.P., Chovanec, P., Plaza Reyes, A., Petropoulos, S., Corcoran, A.E., Walker, R., Douagi, I., Lanner, F. & Rugg-Gunn, P.J. (2017) Comprehensive Cell Surface Protein Profiling Identifies Specific Markers of Human Naive and Primed Pluripotent States. *Cell Stem Cell*. 20 (6), 874-890.e7. doi:10.1016/j.stem.2017.02.014.
- de Dieuleveult, M., Yen, K., Hmitou, I., Depaux, A., Boussouar, F., et al. (2016) Genome-wide nucleosome specificity and function of chromatin remodelers in ES cells. *Nature*. 530 (7588), 113–116. doi:10.1038/nature16505.

Drivas, T.G., Li, D., Nair, D., Alaimo, J.T., Alders, M., et al. (2020) A second cohort of CHD3 patients expands the molecular mechanisms known to cause Snijders Blok-Campeau syndrome. *European Journal of Human Genetics*. 28 (10), 1422–1431. doi:10.1038/s41431-020-0654-4.

Ee, L.-S., McCannell, K.N., Tang, Y., Fernandes, N., Hardy, W.R., Green, M.R., Chu, F. & Fazzio, T.G. (2017) An Embryonic Stem Cell-Specific NuRD Complex Functions through Interaction with WDR5. *Stem Cell Reports*. 8 (6), 1488–1496. doi:10.1016/j.stemcr.2017.04.020.

Egan, C.M., Nyman, U., Skotte, J., Streubel, G., Turner, S., O'Connell, D.J., Rraklli, V., Dolan, M.J., Chadderton, N., Hansen, K., Farrar, G.J., Helin, K., Holmberg, J. & Bracken, A.P. (2013) CHD5 Is Required for Neurogenesis and Has a Dual Role in Facilitating Gene Expression and Polycomb Gene Repression. *Developmental Cell*. 26 (3), 223–236. doi:10.1016/j.devcel.2013.07.008.

Ganger, M.T., Dietz, G.D. & Ewing, S.J. (2017) A common base method for analysis of qPCR data and the application of simple blocking in qPCR experiments. *BMC Bioinformatics*. 18 (1), 534. doi:10.1186/s12859-017-1949-5.

Hirota, A., Nakajima-Koyama, M., Ashida, Y. & Nishida, E. (2019) The nucleosome remodeling and deacetylase complex protein CHD4 regulates neural differentiation of mouse embryonic stem cells by down-regulating p53. *Journal of Biological Chemistry*. 294 (1), 195–209. doi:10.1074/jbc.RA118.004086.

Hoffmann, A. & Spengler, D. (2019) Chromatin Remodeling Complex NuRD in Neurodevelopment and Neurodevelopmental Disorders. *Frontiers in Genetics*. 10. doi:10.3389/fgene.2019.00682.

Huang, Y., Zhang, H., Wang, L., Tang, C., Qin, X., et al. (2020) JMJD3 acts in tandem with KLF4 to facilitate reprogramming to pluripotency. *Nature Communications*. 11 (1), 5061. doi:10.1038/s41467-020-18900-z.

King, N.M. & Perrin, J. (2014) Ethical issues in stem cell research and therapy. *Stem Cell Research & Therapy*. 5 (4), 85. doi:10.1186/scrt474.

Lai, A.Y. & Wade, P.A. (2011) Cancer biology and NuRD: a multifaceted chromatin remodelling complex. *Nature Reviews Cancer*. 11 (8), 588–596. doi:10.1038/nrc3091.

Lai, T.-Y., Cao, J., Ou-Yang, P., Tsai, C.-Y., Lin, C.-W., Chen, C.-C., Tsai, M.-K. & Lee, C.-Y. (2022) Different methods of detaching adherent cells and their effects on the cell surface expression of Fas receptor and Fas ligand. *Scientific Reports*. 12 (1), 5713. doi:10.1038/s41598-022-09605-y.

Lancaster, M.A. & Knoblich, J.A. (2014) Generation of cerebral organoids from human pluripotent stem cells. *Nature Protocols*. 9 (10), 2329–2340.  
doi:10.1038/nprot.2014.158.

Lanctot, P.M., Gage, F.H. & Varki, A.P. (2007) The glycans of stem cells. *Current Opinion in Chemical Biology*. 11 (4), 373–380. doi:10.1016/j.cbpa.2007.05.032.

Laut, A.K., Dorneburg, C., Fürstberger, A., Barth, T.F.E., Kestler, H.A., Debatin, K.-M. & Beltinger, C. (2022) CHD5 inhibits metastasis of neuroblastoma. *Oncogene*. 41 (5), 622–633. doi:10.1038/s41388-021-02081-0.

Le Gallo, M., O'Hara, A.J., Rudd, M.L., Urick, M.E., Hansen, N.F., O'Neil, N.J., Price, J.C., Zhang, S., England, B.M., Godwin, A.K., Sgroi, D.C., Hieter, P., Mullikin, J.C., Merino, M.J. & Bell, D.W. (2012) Exome sequencing of serous endometrial tumors identifies recurrent somatic mutations in chromatin-remodeling and ubiquitin ligase complex genes. *Nature Genetics*. 44 (12), 1310–1315. doi:10.1038/ng.2455.

Liu, L.-P. & Zheng, Y.-W. (2019) Predicting differentiation potential of human pluripotent stem cells: Possibilities and challenges. *World Journal of Stem Cells*. 11 (7), 375–382. doi:10.4252/wjsc.v11.i7.375.

Low, J.K.K., Webb, S.R., Silva, A.P.G., Saathoff, H., Ryan, D.P., Torrado, M., Brofelth, M., Parker, B.L., Shepherd, N.E. & Mackay, J.P. (2016) CHD4 Is a Peripheral Component of the Nucleosome Remodeling and Deacetylase Complex\*. *Journal of Biological Chemistry*. 291 (30), 15853–15866. doi:10.1074/jbc.M115.707018.

Lu, X., Zhang, M., Li, G., Zhang, S., Zhang, J., Fu, X. & Sun, F. (2023) Applications and Research Advances in the Delivery of CRISPR/Cas9 Systems for the Treatment of Inherited Diseases. *International Journal of Molecular Sciences*. 24 (17), 13202. doi:10.3390/ijms241713202.

Miller, A., Ralser, M., Kloet, S.L., Loos, R., Nishinakamura, R., Bertone, P., Vermeulen, M. & Hendrich, B. (2016) Sall4 controls differentiation of pluripotent cells independently of the Nucleosome Remodelling and Deacetylation (NuRD) complex. *Development*. 143 (17), 3074–3084. doi:10.1242/dev.139113.

Miyoshi, K., Tsuji, D., Kudoh, K., Satomura, K., Muto, T., Itoh, K. & Noma, T. (2010) Generation of human induced pluripotent stem cells from oral mucosa. *Journal of Bioscience and Bioengineering*. 110 (3), 345–350. doi:10.1016/j.jbiosc.2010.03.004.

Musselman, C.A., Ramírez, J., Sims, J.K., Mansfield, R.E., Oliver, S.S., Denu, J.M., Mackay, J.P., Wade, P.A., Hagman, J. & Kutateladze, T.G. (2012) Bivalent recognition

of nucleosomes by the tandem PHD fingers of the CHD4 ATPase is required for CHD4-mediated repression. *Proceedings of the National Academy of Sciences*. 109 (3), 787–792. doi:10.1073/pnas.1113655109.

Nelakanti, R.V., Kooreman, N.G. & Wu, J.C. (2015) Teratoma Formation: A Tool for Monitoring Pluripotency in Stem Cell Research. *Current protocols in stem cell biology*. 32, 4A.8.1-4A.8.17. doi:10.1002/9780470151808.sc04a08s32.

Nitarska, J., Smith, J.G., Sherlock, W.T., Hillege, M.M.G., Nott, A., Barshop, W.D., Vashisht, A.A., Wohlschlegel, J.A., Mitter, R. & Riccio, A. (2016) A Functional Switch of NuRD Chromatin Remodeling Complex Subunits Regulates Mouse Cortical Development. *Cell Reports*. 17 (6), 1683–1698. doi:10.1016/j.celrep.2016.10.022.

Pagliaroli, L., Porazzi, P., Curtis, A.T., Scopa, C., Mikkers, H.M.M., Freund, C., Daxinger, L., Deliard, S., Welsh, S.A., Offley, S., Ott, C.A., Calabretta, B., Brugmann, S.A., Santen, G.W.E. & Trizzino, M. (2021) Inability to switch from ARID1A-BAF to ARID1B-BAF impairs exit from pluripotency and commitment towards neural crest formation in ARID1B-related neurodevelopmental disorders. *Nature Communications*. 12 (1), 6469. doi:10.1038/s41467-021-26810-x.

Parenti, I., Lehalle, D., Nava, C., Torti, E., Leitão, E., et al. (2021) Missense and truncating variants in CHD5 in a dominant neurodevelopmental disorder with intellectual disability, behavioral disturbances, and epilepsy. *Human Genetics*. 140 (7), 1109–1120. doi:10.1007/s00439-021-02283-2.

Park, I.-H., Zhao, R., West, J.A., Yabuuchi, A., Huo, H., Ince, T.A., Lerou, P.H., Lensch, M.W. & Daley, G.Q. (2008) Reprogramming of human somatic cells to pluripotency with defined factors. *Nature*. 451 (7175), 141–146. doi:10.1038/nature06534.

Pascual, P., Tenorio-Castano, J., Mignot, C., Afenjar, A., Arias, P., et al. (2023) Snijders Blok–Campeau Syndrome: Description of 20 Additional Individuals with Variants in CHD3 and Literature Review. *Genes*. 14 (9), 1664. doi:10.3390/genes14091664.

Pomeroy, J.E., Hough, S.R., Davidson, K.C., Quaas, A.M., Rees, J.A. & Pera, M.F. (2016) Stem Cell Surface Marker Expression Defines Late Stages of Reprogramming to Pluripotency in Human Fibroblasts. *Stem Cells Translational Medicine*. 5 (7), 870–882. doi:10.5966/sctm.2015-0250.

Prescott, S.L., Srinivasan, R., Marchetto, M.C., Grishina, I., Narvaiza, I., Selleri, L., Gage, F.H., Swigut, T. & Wysocka, J. (2015) Enhancer Divergence and cis-Regulatory

Evolution in the Human and Chimp Neural Crest. *Cell.* 163 (1), 68–83.  
doi:10.1016/j.cell.2015.08.036.

Scimone, M.L., Meisel, J. & Reddien, P.W. (2010) The Mi-2-like Smed-CHD4 gene is required for stem cell differentiation in the planarian Schmidtea mediterranea. *Development (Cambridge, England).* 137 (8), 1231–1241. doi:10.1242/dev.042051.

Seto, E. & Yoshida, M. (2014) Erasers of Histone Acetylation: The Histone Deacetylase Enzymes. *Cold Spring Harbor Perspectives in Biology.* 6 (4), a018713.  
doi:10.1101/cshperspect.a018713.

Shihan, M.H., Novo, S.G., Le Marchand, S.J., Wang, Y. & Duncan, M.K. (2021) A simple method for quantitating confocal fluorescent images. *Biochemistry and Biophysics Reports.* 25, 100916. doi:10.1016/j.bbrep.2021.100916.

Siismets, E.M. & Hatch, N.E. (2020) Cranial Neural Crest Cells and Their Role in the Pathogenesis of Craniofacial Anomalies and Coronal Craniosynostosis. *Journal of Developmental Biology.* 8 (3), 18. doi:10.3390/jdb8030018.

Simicevic, J. & Deplancke, B. (2017) Transcription factor proteomics—Tools, applications, and challenges. *PROTEOMICS.* 17 (3–4), 1600317.  
doi:10.1002/pmic.201600317.

Snijders Blok, L., Rousseau, J., Twist, J., Ehresmann, S., Takaku, M., et al. (2018) CHD3 helicase domain mutations cause a neurodevelopmental syndrome with macrocephaly and impaired speech and language. *Nature Communications.* 9 (1), 4619.  
doi:10.1038/s41467-018-06014-6.

Takahashi, K., Tanabe, K., Ohnuki, M., Narita, M., Ichisaka, T., Tomoda, K. & Yamanaka, S. (2007) Induction of Pluripotent Stem Cells from Adult Human Fibroblasts by Defined Factors. *Cell.* 131 (5), 861–872. doi:10.1016/j.cell.2007.11.019.

Takahashi, K. & Yamanaka, S. (2006) Induction of Pluripotent Stem Cells from Mouse Embryonic and Adult Fibroblast Cultures by Defined Factors. *Cell.* 126 (4), 663–676.  
doi:10.1016/j.cell.2006.07.024.

Takata, K., Saito, K., Maruyama, S., Miyata-Takata, T., Iioka, H., Okuda, S., Ling, Y., Karube, K., Miki, Y., Maeda, Y., Yoshino, T., Steidl, C. & Kondo, E. (2019) Identification of TRA-1-60-positive cells as a potent refractory population in follicular lymphomas. *Cancer Science.* 110 (1), 443–457. doi:10.1111/cas.13870.

Temple, S. (2001) The development of neural stem cells. *Nature.* 414 (6859), 112–117.  
doi:10.1038/35102174.

Torchy, M.P., Hamiche, A. & Klaholz, B.P. (2015) Structure and function insights into the NuRD chromatin remodeling complex. *Cellular and Molecular Life Sciences*. 72 (13), 2491–2507. doi:10.1007/s00018-015-1880-8.

Turner, D.A., Hayward, P.C., Baillie-Johnson, P., Rué, P., Broome, R., Faunes, F. & Martinez Arias, A. (2014) Wnt/β-catenin and FGF signalling direct the specification and maintenance of a neuromesodermal axial progenitor in ensembles of mouse embryonic stem cells. *Development (Cambridge, England)*. 141 (22), 4243–4253. doi:10.1242/dev.112979.

Wang, H.-B. & Zhang, Y. (2001) Mi2, an auto-antigen for dermatomyositis, is an ATP-dependent nucleosome remodeling factor. *Nucleic Acids Research*. 29 (12), 2517–2521.

Wang, Z., Oron, E., Nelson, B., Razis, S. & Ivanova, N. (2012) Distinct Lineage Specification Roles for NANOG, OCT4, and SOX2 in Human Embryonic Stem Cells. *Cell Stem Cell*. 10 (4), 440–454. doi:10.1016/j.stem.2012.02.016.

Watabe, T. & Miyazono, K. (2009) Roles of TGF-β family signaling in stem cell renewal and differentiation. *Cell Research*. 19 (1), 103–115. doi:10.1038/cr.2008.323.

Woodage, T., Basrai, M.A., Baxevanis, A.D., Hieter, P. & Collins, F.S. (1997) Characterization of the CHD family of proteins. *Proceedings of the National Academy of Sciences*. 94 (21), 11472–11477. doi:10.1073/pnas.94.21.11472.

Xue, Y., Wong, J., Moreno, G.T., Young, M.K., Côté, J. & Wang, W. (1998) NURD, a Novel Complex with Both ATP-Dependent Chromatin-Remodeling and Histone Deacetylase Activities. *Molecular Cell*. 2 (6), 851–861. doi:10.1016/S1097-2765(00)80299-3.

Ye, L., Swingen, C. & Zhang, J. (2013) Induced Pluripotent Stem Cells and Their Potential for Basic and Clinical Sciences. *Current Cardiology Reviews*. 9 (1), 63–72. doi:10.2174/157340313805076278.

Ye, Z., Zhan, H., Mali, P., Dowey, S., Williams, D.M., Jang, Y.-Y., Dang, C.V., Spivak, J.L., Moliterno, A.R. & Cheng, L. (2009) Human-induced pluripotent stem cells from blood cells of healthy donors and patients with acquired blood disorders. *Blood*. 114 (27), 5473–5480. doi:10.1182/blood-2009-04-217406.

Yu, J., Hu, K., Smuga-Otto, K., Tian, S., Stewart, R., Slukvin, I.I. & Thomson, J.A. (2009) Human Induced Pluripotent Stem Cells Free of Vector and Transgene Sequences. *Science*. 324 (5928), 797–801. doi:10.1126/science.1172482.

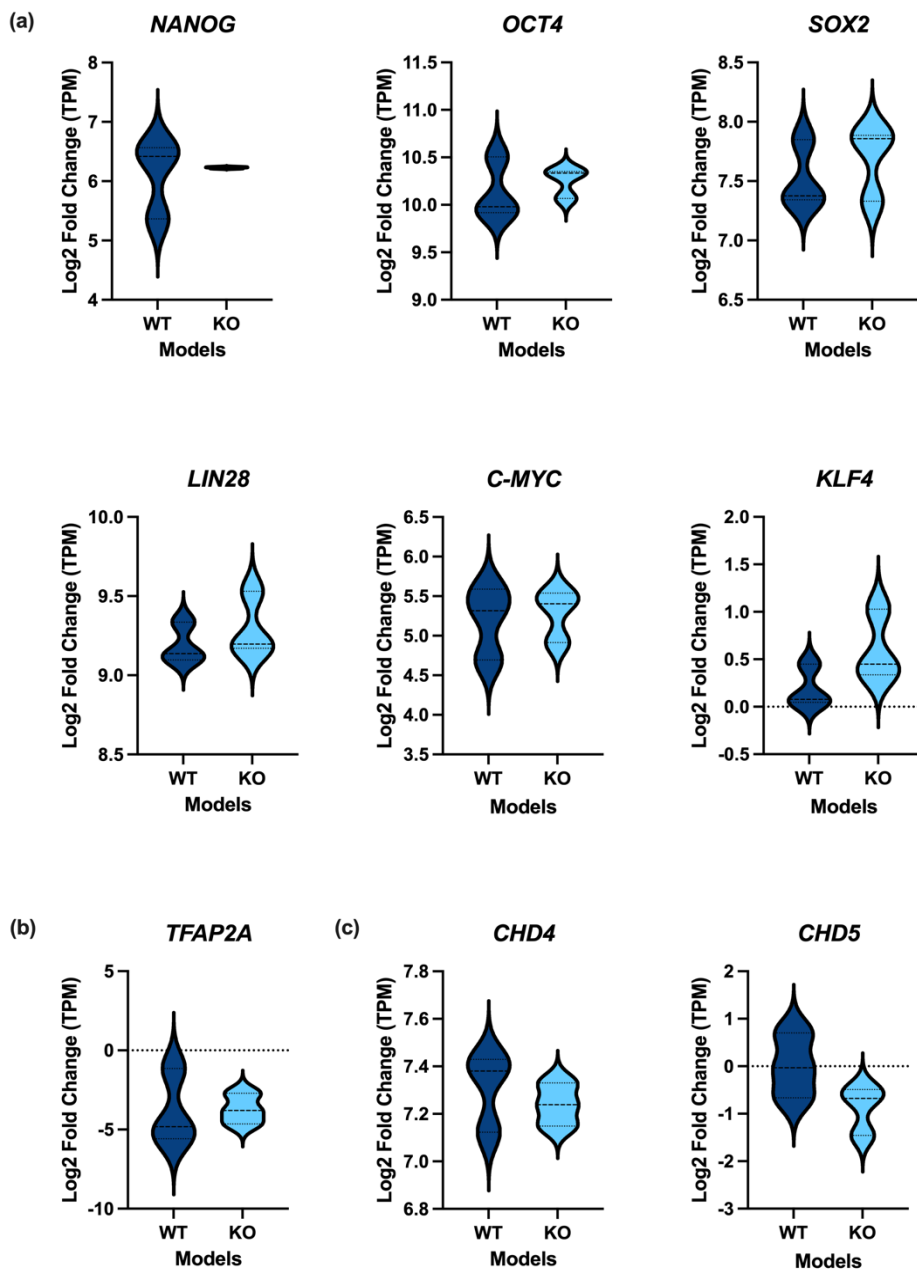
Yu, J., Vodyanik, M.A., Smuga-Otto, K., Antosiewicz-Bourget, J., Frane, J.L., Tian, S., Nie, J., Jonsdottir, G.A., Ruotti, V., Stewart, R., Slukvin, I.I. & Thomson, J.A. (2007) Induced Pluripotent Stem Cell Lines Derived from Human Somatic Cells. *Science*. 318 (5858), 1917–1920. doi:10.1126/science.1151526.

Zalc, A., Sinha, R., Gulati, G.S., Wesche, D.J., Daszczuk, P., Swigut, T., Weissman, I.L. & Wysocka, J. (2021) Reactivation of the pluripotency program precedes formation of the cranial neural crest. *Science (New York, N.Y.)*. 371 (6529), eabb4776. doi:10.1126/science.abb4776.

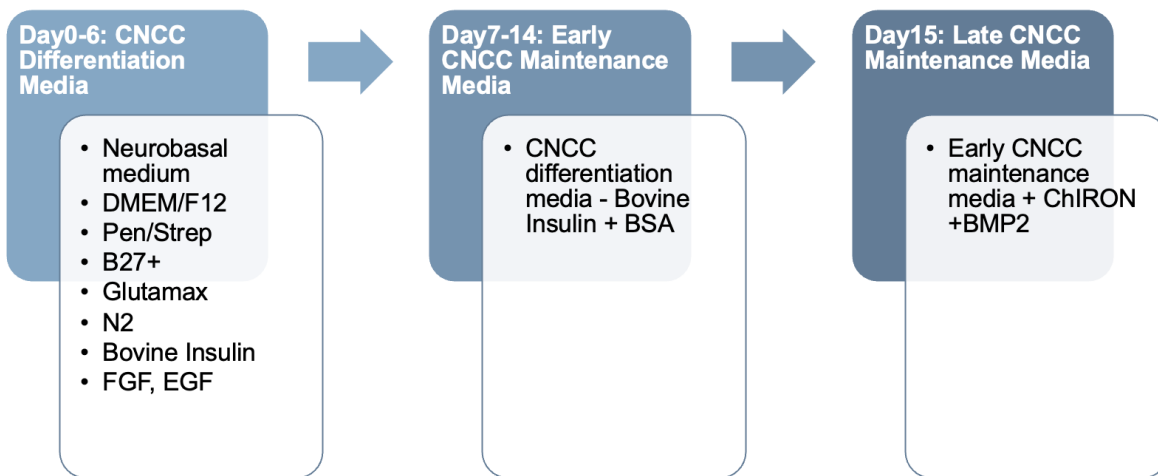
Zhang, W., Aubert, A., Gomez de Segura, J.M., Karuppasamy, M., Basu, S., et al. (2016) The Nucleosome Remodeling and Deacetylase Complex NuRD Is Built from Preformed Catalytically Active Sub-modules. *Journal of Molecular Biology*. 428 (14), 2931–2942. doi:10.1016/j.jmb.2016.04.025.

Zhao, H., Han, Z., Liu, X., Gu, J., Tang, F., Wei, G. & Jin, Y. (2017) The chromatin remodeler Chd4 maintains embryonic stem cell identity by controlling pluripotency-and differentiation-associated genes. *The Journal of Biological Chemistry*. 292 (20), 8507–8519. doi:10.1074/jbc.M116.770248.

## Supplementary Materials



**Supplementary Figure 1. The violin plots for RNA-Seq log2 gene expression fold change for (a) pluripotency marker genes, (b) differentiation marker gene, (c) CHD4 and CHD5.** There is no significant difference between CHD3-WT and CHD3-KO models for all of the genes shown. Statistical test adapted was the Unpaired Students' t-test. Unequal variance assumption was made for all genes except equal variance assumption was conducted for NANOG. Two- tail analysis was applied to all genes except one-tail analysis was applied for CHD4/5. Dark blue represents CHD3-WT iPSC model while light blue represents CHD3-KO iPSC model. TPM was the normalization method applied for relative abundance of transcripts in the reads.



**Supplementary Figure 2. Prescott et al., 2015 iPSCs-CNCCs differentiation protocol.** The whole differentiation takes around 18 days. The differentiation requires CNCC differentiation media (day0-6), early (day7-14) and late CNCC maintenance media (day15-). The mechanism behind is to differentiate the iPSCs into neuroectoderm and then into CNCCs.